The Journal of Chemical Physics

Quantum optimal control of multiple weakly interacting molecular rotors in the time-dependent Hartree approximation

Cite as: J. Chem. Phys. **150**, 164303 (2019); https://doi.org/10.1063/1.5091520
Submitted: 02 February 2019 . Accepted: 03 April 2019 . Published Online: 23 April 2019

Alicia Magann, Linhan Chen, Tak-San Ho, and Herschel Rabitz

The Journal of Chemical Physics ARTICLE scitation.org/journal/jcp

Quantum optimal control of multiple weakly interacting molecular rotors in the time-dependent Hartree approximation

Cite as: J. Chem. Phys. 150, 164303 (2019); doi: 10.1063/1.5091520
Submitted: 2 February 2019 • Accepted: 3 April 2019 •
Published Online: 22 April 2019

Alicia Magann,[1,a] Linhan Chen,[2] Tak-San Ho,[3] and Herschel Rabitz[3,b]

AFFILIATIONS

[1]Department of Chemical and Biological Engineering, Princeton University, Princeton, New Jersey 08544, USA
[2]Department of Physics, Princeton University, Princeton, New Jersey 08544, USA
[3]Department of Chemistry, Princeton University, Princeton, New Jersey 08544, USA

[a]Electronic mail: amagann@princeton.edu
[b]Electronic mail: hrabitz@princeton.edu

ABSTRACT

We perform quantum optimal control simulations, based on the Time-Dependent Hartree (TDH) approximation, for systems of three to five dipole-dipole coupled OCS rotors. A control electric field is used to steer all of the individual rotors, arranged in chains and regular polygons in a plane, toward either identical or unique objectives. The goal is to explore the utility of the TDH approximation to model the field-induced dynamics of multiple interacting rotors in the weak dipole-dipole coupling regime. A stochastic hill climbing approach is employed to seek an optimal control field that achieves the desired objectives at a specified target time. We first show that multiple rotors in chain and polygon geometries can be identically oriented in the same direction; these cases do not significantly depend on the presence of the dipole-dipole interaction. Additionally, in particular geometrical arrangements, we demonstrate that individual rotors can be uniquely manipulated toward different objectives with the same field. Specifically, it is shown that for a three rotor chain, the two end rotors can be identically oriented in a specific direction while keeping the middle rotor in its ground state, and for an equilateral triangle, two rotors can be identically oriented in a specific direction while the third rotor is oriented in the opposite direction. These multirotor unique objective cases exploit the shape of the field in coordination with dipole-dipole coupling between the rotors. Comparisons to numerically exact calculations, utilizing the TDH-determined fields, are given for all optimal control studies involving systems of three rotors.

I. INTRODUCTION

There is significant interest in the ability to steer the dynamics of a quantum system in a desired way using optimally shaped fields. One approach for designing these fields is quantum optimal control.[1] There are growing numbers of applications of quantum optimal control methods including high harmonic generation,[2] quantum information processing,[3,4] the control of selective vibrational mode excitation,[5] and the control of chemical reactions.[6–8] However, while a significant body of literature concerning quantum control has been developed in recent decades,[1] only a small fraction of theoretical work considers the control of systems with many interacting degrees of freedom. The goal of this paper is to make a contribution in this important area. To this end, we explore the utility of the Time-Dependent Hartree (TDH) approximation[9,10] for modeling the field-induced dynamics of interacting molecular rotors in the weak dipole-dipole coupling regime, in combination with a derivative-free stochastic hill climbing approach[11,12] for seeking optimal control fields that achieve the desired objectives.

Various theoretical and computational methods have been developed to address the many-body molecular control challenge. Early efforts in the weak field regime involved Gaussian wavepacket approaches[13] as well as applications of the TDH approximation[9,10] to model the control of the dynamics of I_2 coupled to a bath. Later, the Multiconfigurational Time-Dependent Hartree (MCTDH) approach, which improves upon TDH at increased computational expense (see Sec. II B), was also combined with optimal

control theory[14] (e.g., to simulate the control of the vibrational dynamics of pyrazine[15]). Outside the realm of control, early studies applied TDH to nuclear physics problems (e.g., modeling the dynamics of heavy ion collisions[16,17]). In the domain of quantum molecular dynamics without control, TDH has been used to model numerous processes including dissociation dynamics of van der Waals complexes[18,19] and gas phase collisions.[20,21]

In quantum control studies, the problem of finding an optimal control field $\varepsilon(t)$, $t \in [0, T]$ to reach a desired target, defined by the expectation value of an observable O at the terminal time, may be cast as the following optimization problem:

$$\max_{\varepsilon(\cdot)} J[T, \varepsilon(\cdot)], \tag{1}$$

where the cost functional $J[T, \varepsilon(\cdot)] \equiv \langle\psi(T)|O|\psi(T)\rangle$ and the system state $|\psi(T)\rangle$ is generally a nonlinear functional of the control field $\varepsilon(t)$. In practice, $J[T, \varepsilon(\cdot)]$ can also include additional penalty terms in order to give preference to certain field characteristics (e.g., smoothness and low fluence). The optimal field $\varepsilon(t)$ that maximizes the objective functional is usually found iteratively, with various local optimization methods developed for this purpose.[22–25] These local optimization methods typically require the calculation of the gradient of the objective functional with respect to the field, $\frac{\delta J[T,\varepsilon(\cdot)]}{\delta\varepsilon(t)}$, and then move along the latter direction of steepest ascent until the gradient becomes virtually zero (i.e., at the optimum). The resultant field $\varepsilon(t)$ is taken as an optimal control for the given objective.

A direct application of gradient-based algorithms consistent with the TDH approximation is computationally expensive because the associated gradient $\frac{\delta J[T,\varepsilon(\cdot)]}{\delta\varepsilon(t)}$ is a complicated expression due to the presence of the nonlinear mean-field potential in the TDH equations as well as in the general MCTDH context. Although the exact gradient expression (i.e., arising from the original many-body Schrödinger equation) can be utilized for computing an approximate TDH gradient, the performance of the method can suffer due to the inconsistency in the underlying optimal control formulation.[26] In our work, we apply a stochastic hill climbing optimization approach[11,12] that does not require the evaluation of the TDH gradient, but the technique is fully consistent with the TDH dynamical equations.

The systems we consider consist of multiple dipole-dipole coupled molecular rotors in a plane, and we seek optimal control fields to mainly manipulate the individual orientation of the rotors such that their dipoles point in particular directions at a specific time $t = T$. The orientation of molecules is important for applications including high harmonic generation[27] and chemical reactions.[28–30] The orientation of dipole-dipole coupled rotors in lattices has also been studied in the context of quantum phase transitions.[31] Quantum control of molecular rotor orientation has been the subject of prior work, where numerically exact models of one to two rotors were considered.[32–37] By invoking the TDH approximation, we are able to extend the study of rotor orientation control to systems consisting of three to five dipole-dipole coupled rotors, which opens the opportunity to consider complex rotor geometries and control objectives. These latter objectives include cases where the goal is either the same for each rotor or uniquely specified for different rotors. The calculations are performed within the regime of validity of the TDH approximation, which is characterized by a rotor-rotor coupling parameter. Additionally, the TDH and exact wave functions are compared using the TDH-determined control fields for cases of three coupled rotors.

The remainder of the paper is organized as follows. Sec. II presents the formulation for quantum control of multirotor systems. We begin by providing a model of dipole-dipole coupled rotors, and the TDH approximation is then presented, followed by a summary of the stochastic hill climbing method[11,12] adopted to the present control field optimization procedure. Section III provides details of the numerical studies, and we close in Sec. IV with conclusions and an outlook on future work.

II. METHODOLOGY

A. Theoretical description

We consider multiple dipole-dipole coupled linear OCS rigid rotors in the weak dipole-dipole coupling regime arranged in either chain or regular polygon configurations in a plane under the influence of a linearly polarized microwave electric field parallel to the plane. The cases shown are illustrative, amongst other multirotor simulations performed, demonstrating the utility of the TDH approximation within its regime of validity. In the laboratory, planar rotor systems, such as those examined here, could be constructed by adsorbing the molecules onto a cold surface or trapping them in a so-called optical lattice created using the interference of suitable laser beams. It has been shown that optical lattices can form arrays of hundreds of microtraps, which would enable the confinement of molecular rotors in two dimensional geometries such as those we consider.[38] Shaped microwave control fields can be created experimentally by modulating the field using an arbitrary waveform generator.[39,40]

Within the electric dipole approximation, the total Hamiltonian for N planar rotors in the presence of a linearly polarized control field $\varepsilon(t)$ is given as

$$H(\varphi_1, \ldots, \varphi_N, t; \{\boldsymbol{R}_{ij}\}, \{\theta_{ij}\}) = \sum_{i=1}^{N} \left[H_i(\varphi_i) - \mu\varepsilon(t)\cos\varphi_i\right] + V(\varphi_1, \ldots, \varphi_N; \{\boldsymbol{R}_{ij}\}, \{\theta_{ij}\}), \tag{2}$$

where $\varphi_i \in [0, 2\pi)$ denotes the rotational angle of the dipole moment of the ith rotor with respect to the direction of the control field $\varepsilon(t)$, linearly polarized along the $\hat{\boldsymbol{x}}$-axis, $H_i(\varphi_i)$ is the corresponding field-free, single-rotor Hamiltonian of the ith rotor, μ is the magnitude of the permanent single rotor dipole moment, and $V(\varphi_1, \ldots, \varphi_N; \{\boldsymbol{R}_{ij}\}, \{\theta_{ij}\})$ is the dipolar interaction between the rotors. In addition, $\boldsymbol{R}_{ij}$ is the separation vector between the ith and jth rotors, $R_0 < R_{ij} < \infty$, $R_{ij} = |\boldsymbol{R}_{ij}|$, $1 \le i < j \le N$, where R_0 is twice the center of mass radius of an individual OCS rotor and $\theta_{ij} = \boldsymbol{R}_{ij} \cdot \hat{\boldsymbol{x}}/R_{ij}$ is the angle between the vector $\boldsymbol{R}_{ij}$ and the $\hat{\boldsymbol{x}}$-axis (see Fig. 1).

The field-free, single-rotor Hamiltonian for the ith rotor is

$$H_i(\varphi_i) = -\frac{\hbar^2}{2I}\frac{\partial^2}{\partial\varphi_i^2}, \tag{3}$$

where I is the moment of inertia of the rotor, while the interaction describing the dipole-dipole coupling between rotors can be written as

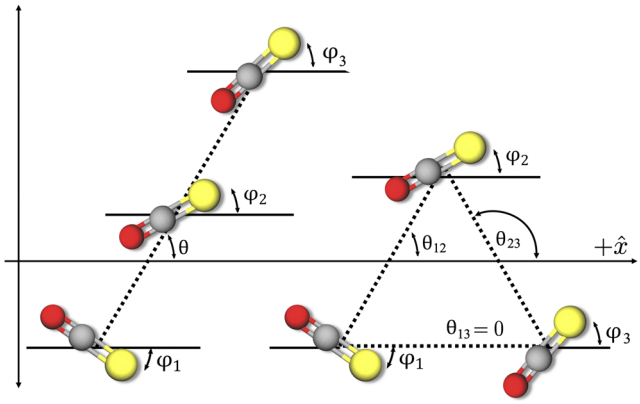

FIG. 1. Diagrams of planar rigid rotors in chain and equilateral triangle configurations. These diagrams will be generalized for other configurations shown later in Sec. III. The rotors point in the directions denoted by φ_i from the $\hat{x}$-axis, while the vector connecting the center of mass of rotors i and j with respect to the $\hat{x}$-axis is denoted θ_{ij}. The control field $\varepsilon(t)$ points along the $\hat{x}$-axis. The molecules are OCS where the color denotes oxygen (red), carbon (gray), and sulfur (yellow).

$$V(\varphi_1,\cdots,\varphi_N;\{\boldsymbol{R}_{ij}\},\{\theta_{ij}\},) = \sum_{1\le i<j\le N}\frac{\mu^2}{4\pi\epsilon_0 R_{ij}^3}\Big\{(1-3\cos^2\theta_{ij})\cos\varphi_i\cos\varphi_j + (1-3\sin^2\theta_{ij})\sin\varphi_i\sin\varphi_j - 3\sin\theta_{ij}\cos\theta_{ij} \times(\cos\varphi_i\sin\varphi_j+\sin\varphi_i\cos\varphi_j)\Big\}, \tag{4}$$

where ϵ_0 is the vacuum permittivity. The dipole moment of OCS is $\mu = 2.36\times10^{-30}$ C m,[41] and its moment of inertia is $I = \frac{\hbar^2}{2B}$, with the rotational constant $B = 4.03\times10^{-24}$ J.[42]

Each coupled rotor system is studied in the basis of the field-free, single-rotor Hamiltonian eigenstates, denoted $|m_i\rangle$, satisfying the eigenvalue equation

$$H_i|m_i\rangle = Bm_i^2|m_i\rangle, \tag{5}$$

where $m_i = -M, -M+1, \ldots, -1, 0, 1, \ldots, M-1, M$. Here and later, we consider a suitably large integer M for each rotor to assure converged results. The eigenstates $|m_i\rangle$ can be expanded as

$$|m_i\rangle = \int_0^{2\pi}|\varphi_i\rangle\langle\varphi_i|m_i\rangle d\varphi_i, \tag{6}$$

where

$$\langle\varphi_i|m_i\rangle = \sqrt{\frac{1}{2\pi}}e^{im_i\varphi_i}, \tag{7}$$

noting that $\int_0^{2\pi}|\varphi_i\rangle\langle\varphi_i|d\varphi_i = 1$. In this basis, the matrix elements of $\cos\varphi_i$ and $\sin\varphi_i$ can be, respectively, written as

$$\langle m_i|\cos\varphi_i|m_i'\rangle = \frac{1}{2}\{\delta_{m_i,m_i'+1}+\delta_{m_i,m_i'-1}\} \tag{8}$$

and

$$\langle m_i|\sin\varphi_i|m_i'\rangle = -\frac{i}{2}\{\delta_{m_i,m_i'+1}-\delta_{m_i,m_i'-1}\}. \tag{9}$$

The state $|\psi(t)\rangle$ describing the dynamics of the rotors is governed by the time-dependent Schrödinger equation

$$i\hbar\frac{\partial}{\partial t}|\psi(t)\rangle = H(\varphi_1,\ldots,\varphi_N,t)|\psi(t)\rangle, \quad |\psi(0)\rangle = |\psi_0\rangle, \tag{10a}$$

which can be re-expressed as the following coupled equations:

$$i\hbar\frac{\partial}{\partial t}c_{m_1\cdots m_N}(t) = \sum_{m_1'}\cdots\sum_{m_N'}\{\langle m_1\cdots m_N|H(t)|m_1'\cdots m_N'\rangle\}c_{m_1'\cdots m_N'}, \tag{10b}$$

after expanding $|\psi(t)\rangle$ as

$$|\psi(t)\rangle = \sum_{m_1=-M}^{M}\cdots\sum_{m_N=-M}^{M}c_{m_1\cdots m_N}(t)|m_1\rangle\ldots|m_N\rangle, \tag{10c}$$

where $H(\varphi_1,\ldots,\varphi_N,t)$ is given in Eq. (2).

B. Time-dependent Hartree approximation

For a quantum system composed of N weakly interacting rotors, the TDH approximation can serve as an effective method for improving the speed and scalability of the calculations to evolve the wave function. Rather than solving the full problem given in Eq. (10b), whose dimension $(2M+1)^N$ scales exponentially in the number of rotors N, the TDH approximation instead solves a set of N coupled single rotor problems and thus scales linearly in the number of rotors, i.e., of the dimension $(2M+1)N$. The TDH equations of motion can be derived by imposing the ansatz

$$|\psi(t)\rangle \approx |\psi_1(t)\rangle|\psi_2(t)\rangle\ldots|\psi_N(t)\rangle, \tag{11}$$

which assumes that the full state $|\psi(t)\rangle$ can be written as a product of single rotor states $|\psi_i(t)\rangle$, $i = 1,\ldots,N$. The MCTDH approach goes beyond this single product formulation by considering multiple coupled products, at the expense of exchanging the linear scaling behavior of TDH for a cost that scales exponentially in the number of degrees of freedom. In this work, the TDH approximation was chosen for N interacting rotors in the weak dipole-dipole coupled regime.

The TDH ansatz in Eq. (11) and the system's Hamiltonian in Eq. (2) can be substituted into the Dirac-Frenkel time-dependent variational principle[43,44] to yield the equations of motion for the single rotor states

$$i\hbar\frac{\partial|\psi_i(t)\rangle}{\partial t} = \Big(H_i(\varphi_i)-\mu\varepsilon(t)\cos\varphi_i + \langle\Phi_i(t)|V(\varphi_1,\ldots,\varphi_N;\{\boldsymbol{R}_{ij}\},\{\theta_{ij}\})|\Phi_i(t)\rangle\Big)|\psi_i(t)\rangle, \tag{12}$$

where $|\Phi_i(t)\rangle = \prod_{k\neq i}|\psi_k(t)\rangle$ and $\langle\Phi_i(t)|V(\varphi_1,\ldots,\varphi_N;\{\boldsymbol{R}_{ij}\},\{\theta_{ij}\})|\Phi_i(t)\rangle$ is the mean-field potential acting on the ith rotor.[45,46]

The validity of the TDH approximation for control simulations of coupled rotors depends on a number of factors, including the strength of the coupling between rotors, the intensity and pulse length of the control field, the separability of the control

objective, and the number of rotors. In our studies, we characterize the strength of coupling between rotors using a dimensionless parameter

$$\Gamma = \max_i \left\{ \Gamma_i \equiv \frac{1}{B} \sum_{\substack{j=1 \\ j \neq i}}^{N} \frac{\mu^2}{4\pi\epsilon_0 R_{ij}^3}, \quad i = 1, \ldots, N \right\}, \tag{13}$$

where Γ_i describes the ratio between the magnitude of the total dipole-dipole potential experienced by rotor i and the rotational constant B, which signifies the energy difference between the ground and the first excited rotational levels of the rotor. The constant Γ can be viewed as the dimensionless characteristic coupling strength over a set of rotors under control. Because the coupling between rotors is given by mean-field potentials, the application of the TDH approximation should work best for systems with weak coupling, characterized by $\Gamma \ll 1$ (i.e., it is exact in the limit of $\Gamma = 0$). As such, in the present work, all simulations are performed using $\Gamma = 0.1$ unless otherwise stated. For systems with stronger coupling, it was found that the TDH mean-field potentials often fail to adequately capture the significant, distinct effects of individual couplings between each pair of rotors upon the system dynamics.

In addition, the difference between the true system Hamiltonian and the TDH approximate Hamiltonian can be considered as a perturbation in the TDH mean-field. Since the error in the solution associated with this perturbation will generally grow with time,[45] the TDH approximation performs best for short control pulses.

Furthermore, the TDH approximation is most useful for analyzing separable control objectives associated with the individual rotors, for example the operator $\cos(\varphi_i + \alpha)$ for rotor i seeking orientation along an angle $\alpha \in [0, 2\pi)$ with respect to the $\hat{\boldsymbol{x}}$-axis. This paper considers single rotor objectives such that the objective functional for the full system can always be decomposed as $J(T) = \sum_i J_i(T)$ for $i = 1, \ldots, N$; however, the dipole-dipole coupling between the rotors can significantly influence $J(T)$. To this end, we analyze two distinct classes of goals: (i) *identical objectives*, where each rotor is steered toward the same target (i.e., the expectation values are sought to satisfy $J_i(T) = J_j(T)$ for all i, j), and (ii) *unique objectives*, where individual rotors are steered toward different targets (i.e., we desire $J_i(T) \neq J_j(T)$ for at least one pair i, j). In examining the evolving dynamics, we will also consider plots of $J_i(t)$ for $t \in [0, T]$.

C. Stochastic hill climbing

In order to design the control fields, we apply a gradient-free stochastic hill climbing optimization approach.[11,12] The trial field $\varepsilon_0(t)$ used to initialize the stochastic hill climbing procedure in all of the optimal control simulations is given as

$$\varepsilon_0(t) = f(t)g(t), \tag{14}$$

where $f(t)$ is a Gaussian envelope function, i.e.,

$$f(t) = \exp\left[-\left(\frac{t - T/2}{T/3} \right)^2 \right], \tag{15}$$

and $g(t)$ is

$$g(t) = a_0\big(0.2\cos(\omega_1 t) + 0.3\cos(\omega_2 t) + 0.5\cos(\omega_3 t)\big), \tag{16}$$

where $a_0 = 4.26 \times 10^3 \frac{\text{V}}{\text{cm}}$ and $\omega_1 = B/\hbar$, $\omega_2 = 3B/\hbar$, and $\omega_3 = 5B/\hbar$ are the first three transition frequencies of the field-free, single-rotor Hamiltonian. The Gaussian envelope $f(t)$ is only imposed on the trial field.

We update the control field at each optimization iteration by stochastically introducing a small perturbation $\delta\varepsilon(t)$ (i.e., discretized over time, where the variation $\delta\varepsilon(t_i)$ in the ith time step is an independent random variable) into the control field and accept the perturbation only if it increases the value of the objective functional such that $J[T, \varepsilon + \delta\varepsilon] > J[T, \varepsilon]$. The perturbations $\{\delta\varepsilon(t_i)\}$ are drawn from a uniform distribution around $\varepsilon(t_i)$ $\forall i$, and the width of the distribution decreases linearly with the distance from the maximum of $J(T)$. Due to the random noise that arises from these stochastic perturbations, we also apply a third order low-pass Butterworth filter with a cutoff frequency of 96 GHz to the control field at each optimization iteration. Finally, we remark that for the first class of *identical* objectives, it is beneficial to initially optimize a field for orienting a single free rotor (FR) and to then use the resultant field as the trial field for the $\Gamma = 0.1$ field optimizations for all configurations. This procedure was found to accelerate the optimization process by ~2 orders of magnitude for every configuration compared with starting from the trial field given in Eq. (14).

III. ILLUSTRATIVE SIMULATIONS

The results presented here will demonstrate that individual rotors (i.e., in systems of N interacting rotors, where $N = 3, 4, 5$, arranged in either chain or regular polygon geometries) can be successfully steered to *identical* as well as *unique* objectives. The identical objective cases in Sec. III A exhibit relatively simple behavior with weak dipole-dipole coupling. These latter cases also serve as an important point of comparison for the unique objective cases that follow in Sec. III B where, despite the dipolar coupling being the same as in Sec. III A, it is shown that suitable fields can be designed to uniquely drive the dynamics of individual rotors.

In all cases, the objective is reached with acceptable quality using a particular control field with a pulse length of $T = 50\hbar/B \approx 1.305$ ns. The total time T is discretized into 1000 equally spaced time points which provided sufficient resolution for the dynamics. The single rotor states are modeled using the basis $m_i = -8, \ldots, -1, 0, 1, \ldots, 8$, which is suitable (i.e., convergence was achieved) for all cases, and each rotor always is initialized in the ground state $|0\rangle$ of its field-free, single-rotor Hamiltonian.

A. Identical objectives

The cases in this subsection involve driving all rotors toward the same orientation in a particular direction. This corresponds to the simultaneous maximization of the expectation values of the individual rotor orientations defined as

$$J_i(T) = \langle \psi_i(T) | \cos(\varphi_i + \alpha) | \psi_i(T) \rangle, \quad i = 1, \ldots, N, \tag{17}$$

where it is understood that the expectation value entails integrating over φ_i and α is the target orientation angle with respect to the $\hat{\boldsymbol{x}}$-axis. For our studies, we choose $\alpha = 0$.

We remark that although the rotors are all driven toward the same objective, depending on their particular spatial arrangement, the rotors themselves are not all identical. For example, for three

rotors in a chain with equal spacing between adjacent rotors, the two end rotors will always be oriented identically with respect to the $\hat{\boldsymbol{x}}$-axis due to the symmetry of the chain, while the middle rotor will be physically different; these distinctions arise from the particular location of a rotor with respect to its neighbors and the resultant impact this has on the dipolar couplings involved. The examples below will illustrate three cases of identical rotor objectives.

1. Case 1: Three rotors in a chain with identical objectives

We begin by considering a chain of three rotors (see Fig. 2). The control field shown in Fig. 2(a) simultaneously maximizes the expectation values of the orientations of three rotors in a chain spaced evenly by $R = 6.29$ nm, corresponding to $\Gamma = 0.1$. Each single rotor objective reaches $J_i(T) = \langle\psi_i(T)|\cos(\varphi_i)|\psi_i(T)\rangle \geq 0.98$ for $i = 1, 2, 3$, which requires the involvement of many eigenstates of the field-free, single rotor Hamiltonians (see Fig. 4). This is reflected in Fig. 2(b), where toward the end of the control interval, the expectation value $J_i(t) = \langle\psi_i(t)|\cos(\varphi_i)|\psi_i(t)\rangle$ displays a distinctive recurrence of sharp peaks and troughs, with peak-to-peak separation equal to the rotational period $2\pi/B \approx 0.164$ ns.

In Fig. 2(b), the TDH mean-field dynamics (solid black curve) are compared against the corresponding exact dynamics with the TDH-determined field (dashed-dotted red curve), and the agreement between them is excellent (with a root mean squared error of $\sqrt{\sum_{i=1}^{1000}\frac{(J_{\text{exact}}(t_i)-J_{\text{TDH}}(t_i))^2}{1000}} = 0.027$) over the course of the entire pulse. In particular, at the terminal time $t = T$, the field gives

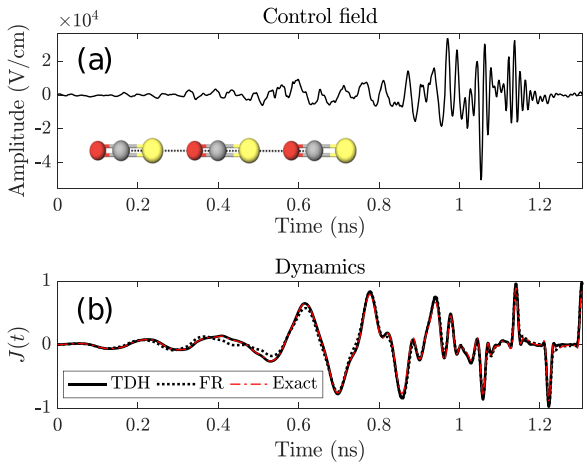

FIG. 2. (a) The optimal control field is shown that orients a chain of three rotors placed along the $\hat{\boldsymbol{x}}$-axis to point in the $+\hat{\boldsymbol{x}}$ direction, as indicated pictorially. (b) The expectation value as a function of time for the sum over all three rotors, i.e., $J(t) = \frac{1}{3}\sum_{i=1}^{3}\langle\psi_i(t)|\cos(\varphi_i)|\psi_i(t)\rangle$, taken out to the target time T. The evolution of $J(t)$ modeled in the TDH approximation (solid black curve) is compared with the evolution when the control field is applied to a free rotor (FR) model (dotted black curve) as well as a numerically exact model (dashed-dotted red curve). In these latter two cases (and for similar tests in the paper), the field was determined from the TDH optimization process. The similarity to the free rotor case (dotted black curve) is not surprising, given the rotor center of mass separation of 6.29 nm. However, we will see later that even in such cases, the dipole-dipole interaction can play a crucial role when nonidentical individual rotor goals break the symmetry of the objective.

$J_{\text{TDH}}(T) = 0.98$ and $J_{\text{exact}}(T) = 0.88$, respectively. Moreover, a comparison to a free rotor (FR) model (which neglects all interactions between rotors) shows slightly poorer agreement (with a root mean squared error of 0.053) between the FR dynamics (dotted black curve) and the exact dynamics, especially apparent at early times, although at the terminal time, the FR model reaches $J_{\text{FR}}(T) = 0.98$. These collective findings demonstrate the expected utility of the TDH method to satisfactorily model the dynamics when the dipole-dipole interaction between rotors is weak.

The field shown in Fig. 2(a) is composed of many free rotor transition frequencies. To this end, it is found that after initializing each of the rotors in the ground state $|0\rangle$, we see a ladderlike progression toward higher energy levels as $J(T)$ increases.[33] This is shown in Fig. 3, where the power spectrum of the control field is plotted at different $J(T)$ values during the optimization. Each of the spectral peaks occurs centered at or very close to a free rotor transition frequency (denoted by the dotted lines), indicating that to achieve $J(T) = 0.94$, the dynamics only draws upon the transitions $|0\rangle \to |\pm1\rangle \to |\pm2\rangle \to |\pm3\rangle \to |\pm4\rangle$. To achieve even higher $J(T)$ values, more transition frequencies involving higher rotational levels appear in the control field. For example, seven transition frequencies are present in the control field for $J(T) = 0.98$, indicating the involvement of the 15 lowest free rotor states $|0\rangle, |\pm1\rangle, \ldots, |\pm7\rangle$. This behavior is also evident in Fig. 4, which illustrates how the rotational state populations evolve in time, culminating with the maximally oriented single rotor states formed by $|m\rangle = |0\rangle, \ldots, |\pm7\rangle$ at the terminal time $T = 1.305$ ns. We remark that for a given M, the corresponding maximum expectation value of the individual orientation operator $\cos\varphi_i$ can be readily calculated exactly with the expression $\max J_i(M) = \cos\frac{\pi}{2M+2}$,[36] where max refers to the maximum eigenvalue of $\cos\varphi_i$ when evaluated in the $(2M + 1)$-dimensional space spanned by the free rotor basis states $|-M\rangle, \ldots, |0\rangle, \ldots, |M\rangle$; for example, $\max J_i(4) = 0.95$ and $\max J_i(7) = 0.98$, which are consistent with our findings.

In addition to the case described above, the same target given in Eq. (17) was used for a three rotor chain with a stronger dipole-dipole coupling of $\Gamma = 0.2$, corresponding to a spacing of $R = 5.0$ nm. A field was optimized to reach $J_i(T) = \langle\psi_i(T)|\cos(\varphi_i)|\psi_i(T)\rangle \geq 0.95$,

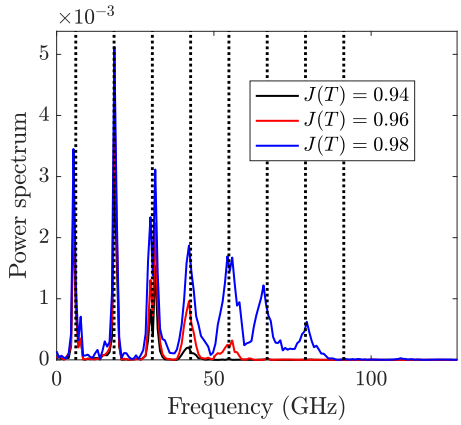

FIG. 3. Power spectrum of evolving control field in units of $V^2/(cm^2\ Hz)$, plotted at the indicated $J(T)$ values during the stochastic hill climbing process.

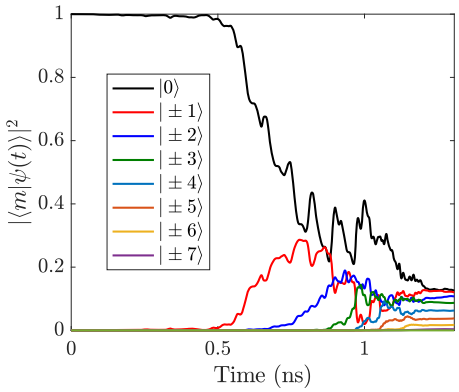

FIG. 4. Time evolution of rotational state populations (averaged over the three rotors) under the influence of the control field given in Fig. 2(a).

for i = 1, 2, and 3. For this stronger coupling case, the TDH approximation resembles the $\Gamma = 0.1$ dynamics at early times, but its performance deteriorates significantly over time, resulting in a smaller exact value $J_{\text{exact}}(T) = 0.64$ at the target time T, compared to $J_{\text{exact}}(T) = 0.88$ for the case shown earlier with $\Gamma = 0.1$. It is evident that the stronger interactions cause the quality of the TDH approximation to deteriorate. This deterioration in the performance of TDH continues with increasing Γ, and this motivated the choice of $\Gamma = 0.1$ coupling for the remainder of examples in the paper.

2. Case 2: Three to five rotors in regular polygons with identical objectives

Here we consider coupled rotors arranged in regular polygon geometries, as depicted in Fig. 5(a), which also includes the optimal control fields designed to steer all rotors to the same objective given in Eq. (17), where N = 3, 4, 5, such that all rotors are ideally identically oriented identically in the $+\hat{\boldsymbol{x}}$ direction at time $t = T$. The rotor spacings for the equilateral triangle, square, and regular pentagon are R = 6.29 nm, R = 6.64 nm, and R = 6.76 nm, respectively, all corresponding to $\Gamma = 0.1$. Note that despite the symmetry of the structures in Fig. 5(a), in some cases, the desired orientations make the rotors inequivalent physically; the scalar dipole-dipole coupling strength index Γ does not include these subtle distinctions. The objective value achieved for each geometry was $J_i(T) = \langle\psi_i(T)|\cos(\varphi_i)|\psi_i(T)\rangle \geq 0.95$ for all i; see Fig. 5(b).

We found that the power spectra (not shown) of these control fields all qualitatively resemble that shown in Fig. 3 for $J(T) = 0.94$, indicating that the fields are composed of the resonant transition frequencies linking the states $|0\rangle$, $|\pm1\rangle$, $|\pm2\rangle$, $|\pm3\rangle$, and $|\pm4\rangle$. Interestingly, although in Fig. 5(b), we found different $J(t)$ behavior at early times depending on the field and geometry, all of the dynamics exhibit the same distinctive recurrence pattern of sharp peaks and troughs at later times, as also found in Fig. 2(b). Finally, when any field in Figs. 5(a) and 2(a), optimized for a given rotor configuration, is applied to one of the other rotor configurations shown pictorially in Figs. 5(a) and 2(a), it still performs remarkably well. In particular, we find that applying the field optimized for the pentagon configuration to the square configuration, and vice versa, results in no drop-off in the objective. On the other hand, the fields optimized for

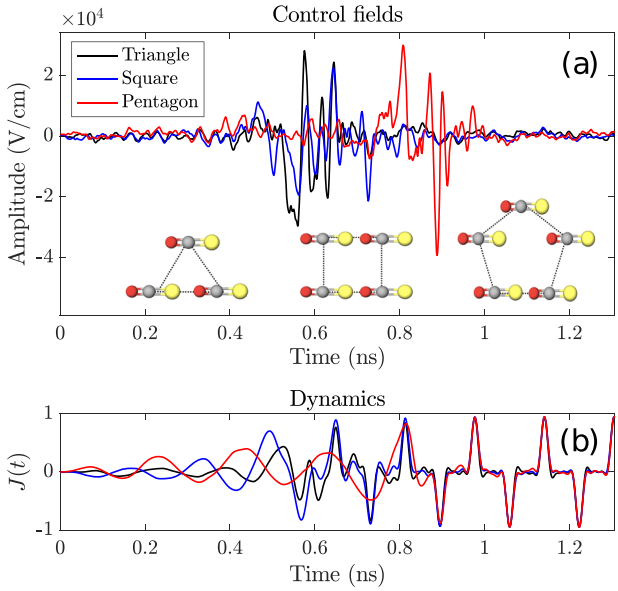

FIG. 5. (a) Each optimal control field (denoted by color) determined to orient all rotors in the $+\hat{\boldsymbol{x}}$ direction arranged correspondingly in either equilateral triangle, square, or regular pentagon configurations. Along with the control fields, the associated control targets are shown pictorially. (b) The expectation values of the N rotors, i.e., $J(t) = \frac{1}{N}\sum_{i=1}^{N=3,4,5}\langle\psi_i(t)|\cos(\varphi_i)|\psi_i(t)\rangle$, are shown for each configuration in (a) with the same color scheme.

polygon configurations were found to perform less satisfactorily in the three rotor chain configuration, with the greatest drop-off occurring when the field optimized to achieve $J_i(T) \geq 0.95$ in the pentagon is tested against the chain, resulting in $J_2(T) = 0.92$ for the middle rotor.

B. Unique objectives

Here we show two cases that highlight the capability of an optimal control field to achieve multiple unique single rotor objectives simultaneously, which can only be attained by the control working "cooperatively" with the dipole-dipole interaction potentials. Thus, these cases behave quite distinctly from those in Sec. III A where the dipole-dipole coupling evidently played a small role.

In the first case, the rotors are arranged in a chain, as in Fig. 2, and in the second case, the rotors are arranged in a triangle, as in the first case of Fig. 5. Reiterating the remark above, although the dipole-dipole coupling is weak in both cases, its presence is the key factor enabling the applied field to have a different control outcome over the individual rotors (i.e., a noninteracting free rotor model would not permit distinct objectives for the different rotors).

1. Case 1: Three rotors in a chain with unique objectives

We seek to identically orient the two end rotors in a chain of three rotors in the $+\hat{\boldsymbol{x}}$ direction while keeping the middle rotor in its ground state $|0\rangle$ at the terminal time $t = T$ (see Fig. 6). The objective for this control target is to maximize the joint expectation value defined as

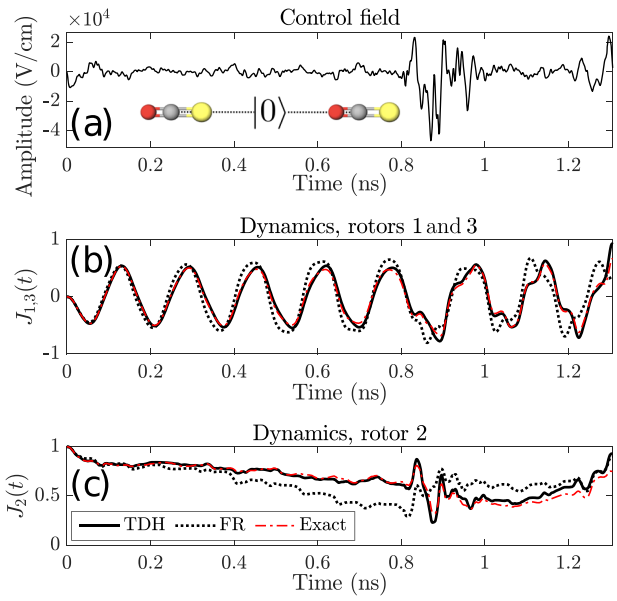

FIG. 6. (a) The optimal control field is shown that seeks to orient the two end rotors in a chain of three in the $+\hat{\boldsymbol{x}}$ direction, while the middle rotor is targeted to be in its ground state $|0\rangle$ at $t = T$. The associated control objective is also shown pictorially. In (b) and (c), the evolution of the orientation expectation value $J_{1,3}(t)$ is plotted for rotors 1 and 3 and the population in the ground state $J_2(t)$ is plotted for rotor 2, respectively. The evolution of $J_{1,3}(t)$ and $J_2(t)$ for the overall system modeled in the TDH approximation (solid black curve) is compared with the evolution when the control field is applied to a free rotor (FR) model (dotted black curve) as well as an exact model (dashed-dotted red curve).

$$J(T) = \langle\psi_1(T)|\cos(\varphi_1)|\psi_1(T)\rangle + \langle\psi_2(T)|0\rangle\langle 0|\psi_2(T)\rangle + \langle\psi_3(T)|\cos(\varphi_3)|\psi_3(T)\rangle = J_1(T) + J_2(T) + J_3(T)\,. \tag{18}$$

Figure 6(a) shows the optimal control field, and Fig. 6(b) shows how the orientation of rotors 1 and 3 evolves toward $J_{1,3}(T) = J_1(T) = J_3(T)$, while the evolution of the population in the state $|0\rangle$ for rotor 2 is shown in Fig. 6(c). It was found that for rotors 1 and 3, the field gives $J_{1,3;\,\mathrm{TDH}}(T) = 0.93$, $J_{1,3;\,\mathrm{exact}}(T) = 0.66$, and $J_{1,3;\,\mathrm{FR}}(T) = 0.35$, while for rotor 2, the field gives $J_{2;\,\mathrm{TDH}}(T) = 0.93$, $J_{2;\,\mathrm{exact}}(T) = 0.75$, and $J_{2;\,\mathrm{FR}}(T) = 0.90$. At the terminal time $t = T$, rotor 2 was primarily lying in the desired state $|0\rangle$, but at intermediate times, rotational states $|\pm1\rangle$ and $|\pm2\rangle$ were also occupied, reflecting the interplay between rotor 2 and rotors 1 and 3 in order for them all to reach their respective targets. Furthermore, rotors 1 and 3, whose orientation is sought, oscillate over time in Fig. 6(b) with a beating structure quite different from that of the linear chain in Fig. 2(b).

This example shows that the control field is able to uniquely address the end rotors and the middle rotor by exploiting the small, but still significant, difference in the dipolar interactions felt by the individual rotors. However, because of the weak dipolar interaction, this control scenario took considerably more optimization iterations (i.e., 1 to 2 orders of magnitude more) than its analog in Fig. 2 where all three rotors are asked to point in the same direction. Naturally, in the present case, three free rotors under the field in Fig. 6(a) would behave identically, rather than as desired; however, $J_{1,3}(t)$ will be distinct from $J_2(t)$ due to the different associated operators in Eq. (18).

2. Case 2: Three rotors in a triangle with unique objectives

For a system of three coupled rotors arranged in a triangle, we seek optimal fields to steer a certain rotor to point in the opposite direction from the other rotors [see the molecular diagram in Fig. 7(a)]. Just as in the prior example involving unique objectives for three rotors in a chain, this was also a challenging control goal to reach. To this end, we have obtained a control field to render $J_i(T) \geq 0.64$ for $i = 1, 2, 3$ for maximizing the following objective:

$$J(T) = \langle\psi_1(T)|\cos(\varphi_1 + \pi)|\psi_1(T)\rangle + \langle\psi_2(T)|\cos(\varphi_2)|\psi_2(T)\rangle + \langle\psi_3(T)|\cos(\varphi_3 + \pi)|\psi_3(T)\rangle = J_1(T) + J_2(T) + J_3(T)\,, \tag{19}$$

with rotor spacing $R = 6.29$ nm, where rotors 1 and 3 are placed along the $\hat{\boldsymbol{x}}$-axis and rotor 2 is placed above them to form an equilateral triangle [see Fig. 7(a)].

As shown in Figs. 7(a)–7(c), the control field is able to successfully drive the rotors to opposing orientations at $t = T$. Specifically, rotors 1 and 3 are oriented in the $-\hat{\boldsymbol{x}}$ direction [Fig. 7(b)] and rotor 2

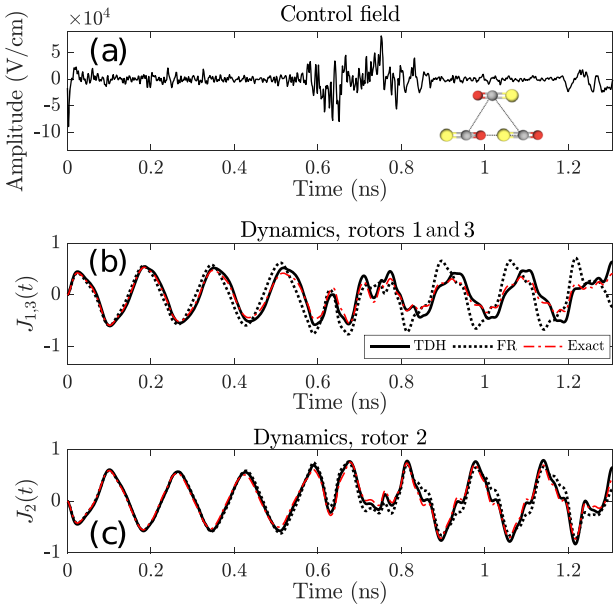

FIG. 7. (a) The optimal control field for orienting rotors arranged in a triangle configuration is shown, where the goal is for rotor 2 (the top rotor) to point in the $+\hat{\boldsymbol{x}}$ direction while rotors 1 and 3 (the bottom rotors) point in the $-\hat{\boldsymbol{x}}$ direction at time $t = T$. The associated control target is also shown pictorially. In (b) and (c), the evolution of the orientation observable expectation value $J_{1,3}(t)$ is plotted for rotors 1 and 3 and $J_2(t)$ for rotor 2, respectively. The evolution of $J_{1,2,3}(t)$ for the overall system modeled in the TDH approximation (solid black curve) is compared with the evolution when the control field is applied to a free rotor (FR) model (dotted black curve) as well as an exact model (dashed-dotted red curve).

is oriented in the $+\hat{\boldsymbol{x}}$ direction [Fig. 7(c)]. It was found that for rotors 1 and 3, the field gives $J_{1,3;\,\mathrm{TDH}}(T) = 0.64$, $J_{1,3;\,\mathrm{exact}}(T) = 0.41$, and $J_{1,3;\,\mathrm{FR}}(T) = -0.23$, while for rotor 2, the field gives $J_{2;\,\mathrm{TDH}}(T) = 0.65$, $J_{2;\,\mathrm{exact}}(T) = 0.41$, and $J_{2;\,\mathrm{FR}}(T) = 0.23$. We remark that the objective values of $J_{1,3;\mathrm{TDH}}(T)$ and $J_{2;\mathrm{TDH}}(T)$ for this control scenario are qualitatively satisfactory but do not approach the optimal value of 1 since the corresponding control objective deals with the demanding physical circumstance of driving very similar rotors toward completely opposite orientations.

The comparison of the TDH dynamics with the corresponding exact dynamics [Figs. 7(b) and 7(c)] reveals that although there is significant deviation present, the behavior of the expectation values $J_{1,2,3}(t)$ drawn from the TDH approximation (solid black curves) is semiquantitatively correct. This is seen in the exact model (dashed-dotted red curves) showing that at $t = T$, the top rotor dominantly points along the $+\hat{\boldsymbol{x}}$ direction, while the bottom two rotors are oriented in the $-\hat{\boldsymbol{x}}$ direction. We also see that the unique objective dynamical evolution is quite distinct from the corresponding triangular case in Fig. 5(b) for the analogous rotors 1 and 3.

Achieving unique objectives for the three rotors was possible because the linearly polarized control field along the $\hat{\boldsymbol{x}}$-axis breaks the symmetry of the dipole-dipole interaction in the rotors' equilateral triangle geometry such that in the presence of the field, rotor 2 feels a different interaction than rotors 1 and 3. However, since the total interaction strength is small ($\Gamma = 0.1$), optimizing a field to exploit this asymmetry proved to be a challenge, with a power spectrum given below in Fig. 8(d) which contains many peaks over a broad spectral range, with most of these peaks shifted away from the free rotor transition frequencies (vertical dotted lines). This is in sharp contrast to the ladderlike power spectrum of a much weaker control field optimized to achieve identical orientations [see Fig. 8(b) and a like situation with three rotors in Figs. 3 and 8(a)].

Finally, as for the identical objective cases, we applied the field optimized for achieving unique objectives in a three rotor chain [Fig. 6(a)], with $J_i(T) \geq 0.93$ to a triangle, to test whether the same unique objectives (i.e., the two end/bottom rotors point in the $+\hat{\boldsymbol{x}}$ direction, while the middle/top rotor is in the ground state) could be reached. It was found that the triangle reaches only $J_{1,3}(T) = \langle\psi_{1,3}(T)|\cos(\varphi_{1,3})|\psi_{1,3}(T)\rangle = 0.57$, indicating a significant drop-off in the expected orientation of the bottom rotors in the $+\hat{\boldsymbol{x}}$ direction; only a slightly lowered ground state population probability of $J_2(T) = \langle\psi_2(T)|0\rangle\langle 0|\psi_2(T)\rangle = 0.90$ was found for the top rotor. Moreover, applying the field optimized for achieving *opposite* orientations in a three rotor triangle [Fig. 7(a)] with $J_i(T) \geq 0.64$) to a three rotor chain was found to cause the orientations of all three rotors in the chain to point in the *same* $-\hat{\boldsymbol{x}}$ direction with $J_{1,3}(T) = \langle\psi_{1,3}(T)|\cos(\varphi_{1,3} + \pi)|\psi_{1,3}(T)\rangle = 0.85$ and $J_2(T) = \langle\psi_2(T)|\cos(\varphi_2)|\psi_2(T)\rangle = -0.84$. These findings show that for the unique objective control cases, differences in the configuration of the rotors can lead to quite different behavior of the field-induced dynamics, thereby demonstrating the significant role played by the dipole-dipole coupling in the spatially distinct configurations.

C. Overall analysis

1. Power spectrum

Figure 8 shows the power spectra associated with the fields designed to achieve identical and nonidentical objectives in systems

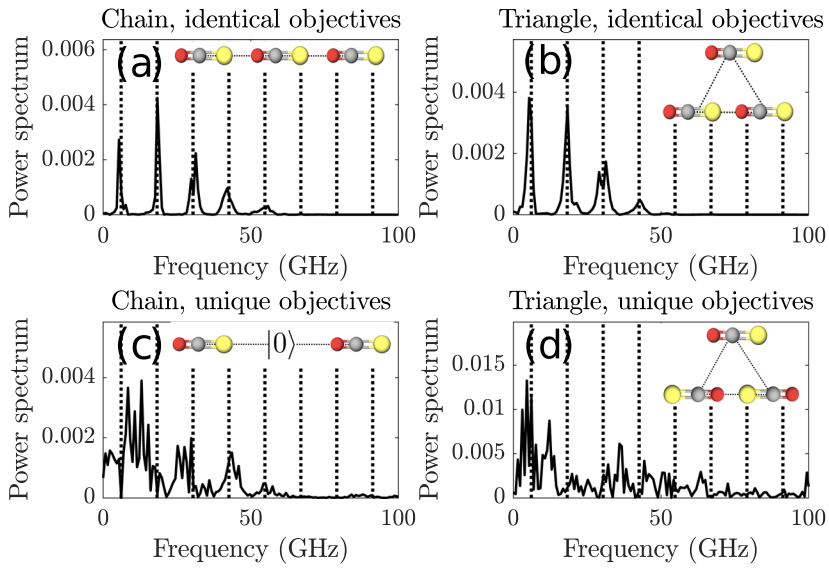

FIG. 8. Power spectra of the optimal control fields designed for systems of three coupled rotors, where the molecular diagram with each spectrum indicates the target that the associated control field aims to achieve. (a) The power spectrum of the field given in Fig. 2 corresponds to the goal of driving three rotors in a chain to point in the $+\hat{\boldsymbol{x}}$ direction. (b) The power spectrum of the field shown in Fig. 5 is presented with the goal to drive all rotors in a triangle to a $+\hat{\boldsymbol{x}}$ orientation. (c) The power spectrum of the field given in Fig. 6 for driving three rotors arranged in a chain to distinct targets (i.e., the two end rotors are targeted to be oriented in the $+\hat{\boldsymbol{x}}$ direction while the middle rotor is in its ground state $|0\rangle$). (d) The power spectrum of the field given in Fig. 7 designed to orient three rotors arranged in a triangle such that the top rotor points in the $+\hat{\boldsymbol{x}}$ direction, while the bottom two rotors point in the $-\hat{\boldsymbol{x}}$ direction. All rotor configurations have a spacing of $R = 6.29$ nm. The dotted lines correspond to the transition frequencies of the field-free, single rotor Hamiltonian. The power spectra are given in units of $\mathrm{V}^2/(\mathrm{cm}^2\,\mathrm{Hz})$.

of three coupled rotors arranged in either a chain or a triangle with a rotor spacing of $R = 6.29$ nm (see Figs. 2 and 5 for the fields to identically orient a chain and a triangle of three rotors, respectively, and Figs. 6 and 7 for the fields to achieve unique objectives in a chain and triangle of three rotors, respectively). The molecular diagrams with each power spectrum indicate the target that the associated control field aims to achieve. Both fields associated with reaching identical objectives have relatively clean power spectra, with peaks situated at or very close to the field-free, single rotor transition frequencies (dotted lines). By contrast, the fields associated with unique objectives have numerous off-resonant peaks, and the field whose power spectrum is given in Fig. 8(d) is also notably stronger than the other three.

2. Comparison of TDH and exact wave functions

Here we compare, respectively, the TDH wave functions of three interacting rotors arranged (i) in a chain and (ii) in a triangle with their exact counterparts (i.e., utilizing the TDH-determined fields) to assess the faithfulness of the TDH approximation to an exact numerical simulation. Specifically, the magnitude of the overlap between the TDH and exact wave functions, as well as the overlap between the free rotor and exact wave functions, is plotted as a function of time for the four cases considered. For both chains and triangles, we analyze cases involving driving all rotors toward identical (orientation) objectives as well as driving all rotors toward unique objectives.

Figure 9(a) shows that the agreement between the TDH and the exact wave function overlaps at the final time for the identical objectives with the chain is $|\langle\psi_{\text{exact}}(T)|\psi_{\text{TDH}}(T)\rangle| = 0.96$ and with the triangle is $|\langle\psi_{\text{exact}}(T)|\psi_{\text{TDH}}(T)\rangle| = 0.86$. The overlap between the free rotor and exact wave functions is lower: $|\langle\psi_{\text{exact}}(T)|\psi_{\text{FR}}(T)\rangle| = 0.87$ for the chain and $|\langle\psi_{\text{exact}}(T)|\psi_{\text{FR}}(T)\rangle| = 0.81$ for the triangle. For the cases with unique objectives in Fig. 9(b), the overlap between the TDH and exact wave functions generally drops more quickly over time such that the overlap is $|\langle\psi_{\text{exact}}(T)|\psi_{\text{TDH}}(T)\rangle| = 0.82$ for the chain and $|\langle\psi_{\text{exact}}(T)|\psi_{\text{TDH}}(T)\rangle| = 0.86$ for the triangle. Likewise, the overlap between the free rotor and exact wave functions drops to $|\langle\psi_{\text{exact}}(T)|\psi_{\text{FR}}(T)\rangle| = 0.74$ for the chain and $|\langle\psi_{\text{exact}}(T)|\psi_{\text{FR}}(T)\rangle| = 0.73$ for the triangle.

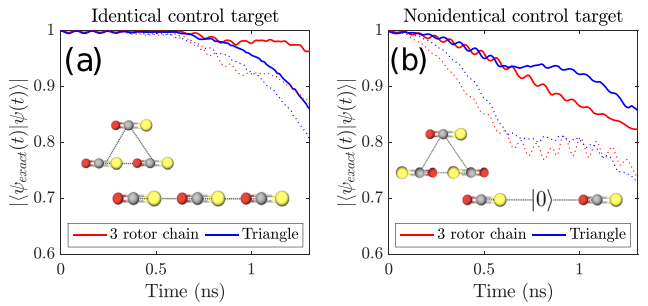

FIG. 9. (a) The overlap is shown between the exact and TDH wave functions (solid lines) as well as the overlap between the exact and free rotor wave functions (dotted lines of corresponding color) for the triangle and the three rotor chain cases when control fields are designed to orient all rotors identically, in the $+\hat{x}$ direction. (b) The overlap between the exact and TDH wave functions (solid lines) as well as the overlap between the exact and free rotor wave functions (dotted lines) for the triangle and three rotor chain cases when control fields are designed to achieve unique control objectives. The pictorial molecular schematics show the control objectives.

Despite the increasing discrepancies over time, the behavior of the TDH wave functions generally mimics that of the exact ones, even for the unique objective cases. This behavior demonstrates that although TDH introduces a distinct level of error, the approximation is able to capture the asymmetric dipolar interaction well enough to design a field capable of addressing rotors individually in a desired manner. Furthermore, as expected, the free rotor approximation fares far worse than the TDH for all four cases shown, with the most significant discrepancies appearing for the unique control objectives.

IV. CONCLUSIONS

We have shown the utility of the TDH approximation to design fields capable of controlling three to five rotors arranged in chain and polygon configurations in the weak dipole-dipole coupling regime. The TDH approximation was successful in modeling the dynamics of multiple interacting rotors and performing the corresponding optimal control simulations in a computationally tractable manner. The first class of illustrations considered orienting all rotors identically, and we found that the search for an optimal field was more challenging for the polygon configurations than for the chain configuration in terms of the number of optimization iterations required. This behavior indicates that, in addition to the coupling strength Γ utilized in this work, the geometry of the rotors is also important for characterizing the dipole-dipole coupling. We also noted that over the course of the stochastic hill climbing field optimization procedure, the field amplitude increased as J rose, accompanied by the emergence of peaks at or close to the free rotor transition frequencies in the power spectra of the optimal fields.

Each of the fields given in Figs. 2(a) and 5(a), optimized to achieve identical objectives in systems of rotors arranged in a three rotor chain, triangle, square, and pentagon, was applied to all rotor arrangements in order to test how well they could orient rotors arranged in geometries other than the one they were specifically optimized for. Due to the weak dipolar coupling, we found that each of the fields performed remarkably well across all geometries considered in this paper. Despite the fields appearing quite distinct over these cases, this outcome indicates a clear degree of robustness of the fields against changes in rotor geometry. Furthermore, all of these fields also did a fair job orienting a single free rotor. This indicates that when high accuracy is not required, fields to attain *identical* objectives in systems of sufficiently weakly coupled rotors could be designed with less computational effort by first considering simpler systems of fewer rotors to determine a good trial field for the desired full set of coupled rotors (e.g., simple chain geometries were found to require fewer field optimization iterations compared with polygon geometries).

We then considered the second class of cases involving simultaneously steering individual rotors toward unique objectives in systems of three coupled rotors. Specifically, we sought to control the orientation of the two end rotors in a chain of three while keeping the middle rotor in its ground rotational state at the final time. In addition, we sought to drive rotors arranged in a triangle geometry to finally have members pointing in opposite orientations. In both cases, we showed that the control field was capable of addressing the

rotors individually, as specified, illustrating the potential for optimally designed pulses to attain complicated objectives that require discrimination between rotors whose Hamiltonians are very similar. The presence of the dipole-dipole coupling term was utilized by the field to reach the discriminatory objectives. Furthermore, we found that the field optimized for achieving unique objectives in a particular rotor configuration (here a three-rotor *chain/triangle*) generally did not lead to the same or even similar unique objective when the original control field was applied to an analogous different rotor configuration (here a three-rotor *triangle/chain*). This finding indicates that there is a strong dependence of the system dynamics on the dipole-dipole coupling expressed through the geometrical arrangement of the rotors for the case of unique objective control.

Our work here involving coupled rotor systems serves as a proof of concept for many body quantum control simulations based on a simple TDH approximation within its realm of validity, and we hope that the findings can serve as the basis for future research. In such studies, different control objectives as well as quantum dynamics approximations beyond TDH could be considered. For example, controlling arrays of trapped, dipole-dipole coupled molecular rotors for quantum computing applications[47–49] could be studied in this context, where quantum dynamics approximations such as TDH could be leveraged to optimize control pulses for implementing quantum logic gates at modest computational expense. These pulses could later serve as trial fields in subsequent optimizations (with an exact model, or directly in the laboratory using learning control) with the goal of efficiently reaching high gate fidelities. Other potential extensions of this work include studies of the controlled orientation of OCS or other linear molecular rotors in novel 3D arrangements,[50] as well as the 3D orientation of systems of weakly coupled symmetric top and asymmetric top molecular rotors. The control of nonidentical rotors could also be examined systematically, as well as nonrotor cases.

ACKNOWLEDGMENTS

A.M. acknowledges support from the DOE CSGF, Grant No. DE-FG02-97ER25308., and L.C. acknowledges support from the Program in Plasma Science and Technology, affiliated with the Princeton Plasma Physics Laboratory. T.-S.H. acknowledges support from Grant No. DOE-DE-FG02-02ER15344, and H.R. acknowledges support from Grant No. ARO W911NF-16-1-0014.

REFERENCES

[1] C. Brif, R. Chakrabarti, and H. Rabitz, "Control of quantum phenomena," in *Advances in Chemical Physics* (John Wiley & Sons, 2011), pp. 1–76.
[2] C. Winterfeldt, C. Spielmann, and G. Gerber, Rev. Mod. Phys. **80**, 117 (2008).
[3] F. Dolde, V. Bergholm, Y. Wang, I. Jakobi, B. Naydenov, S. Pezzagna, J. Meijer, F. Jelezko, P. Neumann, T. Schulte-Herbrüggen, J. Biamonte, and J. Wrachtrup, Nat. Commun. **5**, 3371 (2014).
[4] G. Waldherr, Y. Wang, S. Zaiser, M. Jamali, T. Schulte-Herbrüggen, H. Abe, T. Ohshima, J. Isoya, J. F. Du, P. Neumann, and J. Wrachtrup, Nature **506**, 204 (2014).
[5] L. Liu and J. T. Muckerman, J. Chem. Phys. **107**, 3402 (1997).
[6] D. J. Tannor and S. A. Rice, J. Chem. Phys. **83**, 5013 (1985).
[7] P. Brumer and M. Shapiro, Chem. Phys. Lett. **126**, 541 (1986).
[8] D. G. Abrashkevich, M. Shapiro, and P. Brumer, J. Chem. Phys. **108**, 3585 (1998).
[9] C. S. Guiang and R. E. Wyatt, J. Chem. Phys. **112**, 3580 (2000).
[10] M. Messina, K. R. Wilson, and J. L. Krause, J. Chem. Phys. **104**, 173 (1996).
[11] A. Juels and M. Wattenberg, "Stochastic hillclimbing as a baseline method for evaluating genetic algorithms," in *Advances in Neural Information Processing Systems 8*, edited by D. S. Touretzky, M. C. Mozer, and M. E. Hasselmo (MIT Press, 1996), pp. 430–436.
[12] A. Rosete-Suárez, A. Ochoa-Rodríguez, and M. Sebag, "Automatic graph drawing and stochastic hill climbing," in *Proceedings of the 1st Annual Conference on Genetic and Evolutionary Computation–Volume 2* (Morgan Kaufmann Publishers Inc., 1999), p. 1699.
[13] M. Messina and K. R. Wilson, Chem. Phys. Lett. **241**, 502 (1995).
[14] M. Schröder, J.-L. Carreón-Macedo, and A. Brown, Phys. Chem. Chem. Phys. **10**, 850 (2008).
[15] L. Wang, H.-D. Meyer, and V. May, J. Chem. Phys. **125**, 014102 (2006).
[16] P. Bonche, S. Koonin, and J. W. Negele, Phys. Rev. C **13**, 1226 (1976).
[17] S. Levit, Phys. Rev. C **21**, 1594 (1980).
[18] M. Hernández, A. García-Vela, J. Campos-Martínez, O. Roncero, P. Villarreal, and G. Delgado-Barrio, Comput. Phys. Commun. **145**, 97 (2002).
[19] V. Buch, R. Gerber, and M. Ratner, Chem. Phys. Lett. **101**, 44 (1983).
[20] G. C. Schatz, Chem. Phys. **24**, 263 (1977).
[21] Z. Kirson, R. Gerber, A. Nitzan, and M. Ratner, Surf. Sci. **137**, 527 (1984).
[22] A. Rothman, T.-S. Ho, and H. Rabitz, J. Chem. Phys. **123**, 134104 (2005).
[23] T. Caneva, T. Calarco, and S. Montangero, Phys. Rev. A **84**, 022326 (2011).
[24] Y. Maday and G. Turinici, J. Chem. Phys. **118**, 8191 (2003).
[25] W. Zhu and H. Rabitz, J. Chem. Phys. **109**, 385 (1998).
[26] M. Mundt and D. J. Tannor, New J. Phys. **11**, 105038 (2009).
[27] P. M. Kraus, A. Rupenyan, and H. J. Wörner, Phys. Rev. Lett. **109**, 233903 (2012).
[28] P. R. Brooks, Science **193**, 11 (1976).
[29] R. N. Zare, Science **279**, 1875 (1998).
[30] T. P. Rakitzis, A. J. van den Brom, and M. H. M. Janssen, Science **303**, 1852 (2004).
[31] B. P. Abolins, R. E. Zillich, and K. B. Whaley, J. Chem. Phys. **148**, 102338 (2018).
[32] K. Hoki and Y. Fujimura, Chem. Phys. **267**, 187 (2001).
[33] J. Salomon, C. M. Dion, and G. Turinici, J. Chem. Phys. **123**, 144310 (2005).
[34] G. Turinici and H. Rabitz, J. Phys. A: Math. Theor. **43**, 105303 (2010).
[35] M. Yoshida and Y. Ohtsuki, Chem. Phys. Lett. **633**, 169 (2015).
[36] H. Yu, T.-S. Ho, and H. Rabitz, Phys. Chem. Chem. Phys. **20**, 13008 (2018).
[37] A. Magann, T.-S. Ho, and H. Rabitz, Phys. Rev. A **98**, 043429 (2018).
[38] M. A. Baranov, M. Dalmonte, G. Pupillo, and P. Zoller, Chem. Rev. **112**, 5012 (2012).
[39] J. Yao, Opt. Commun. **284**, 3723 (2011).
[40] I. Lin, J. McKinney, and A. Weiner, IEEE Microwave Wireless Compon. Lett. **15**, 226 (2005).
[41] R. G. Shulman and C. H. Townes, Phys. Rev. **77**, 500 (1950).
[42] A. G. Maki, J. Phys. Chem. Ref. Data **3**, 221 (1974).
[43] P. A. M. Dirac, Math. Proc. Cambridge Philos. Soc. **26**, 376 (1930).
[44] J. Frenkel, *Wave Mechanics* (Clarendon Press, 1934).
[45] R. B. Gerber and M. A. Ratner, "Self-consistent-field methods for vibrational excitations in polyatomic systems," in *Advances in Chemical Physics* (Wiley-Blackwell, 2007), pp. 97–132.
[46] P. Jungwirth and R. B. Gerber, Chem. Rev. **99**, 1583 (1999).
[47] D. DeMille, Phys. Rev. Lett. **88**, 067901 (2002).
[48] L. Bomble, P. Pellegrini, P. Ghesquière, and M. Desouter-Lecomte, Phys. Rev. A **82**, 062323 (2010).
[49] Q. Wei, Y. Cao, S. Kais, B. Friedrich, and D. Herschbach, ChemPhysChem **17**, 3714–3722 (2016).
[50] K. Sharma and B. Friedrich, Phys. Chem. Chem. Phys. **18**, 13467–13477 (2016).